AGU PUBLICATIONS

Geophysical Research Letters

RESEARCH LETTER
10.1002/2015GL065230

**Key Points:**
- Both convection and radial diffusion significantly contribute to transport at transitional energies
- VERB-4D simulations qualitatively agree with observations from tens of keV to MeV
- Convection, radial, pitch angle, energy, and mixed diffusion all play an important role

**Supporting Information:**
- Text S1 and Table S1

**Correspondence to:**
Y. Y. Shprits,
shprits@gmail.com

**Citation:**
Shprits, Y. Y., A. C. Kellerman, A. Y. Drozdov, H. E. Spence, G. D. Reeves, and D. N. Baker (2015), Combined convective and diffusive simulations: VERB-4D comparison with 17 March 2013 Van Allen Probes observations, *Geophys. Res. Lett.*, *42*, 9600–9608, doi:10.1002/2015GL065230.

Received 24 JUL 2015
Accepted 2 SEP 2015
Accepted article online 4 SEP 2015
Published online 19 NOV 2015



# Combined convective and diffusive simulations: VERB-4D comparison with 17 March 2013 Van Allen Probes observations

**Yuri Y. Shprits[1,2], Adam C. Kellerman[1], Alexander Y. Drozdov[1], Harlan E. Spence[3], Geoffrey D. Reeves[4], and Daniel N. Baker[5]**

[1]Department of Earth, Planetary, and Space Sciences, University of California, Los Angeles, California, USA, [2]Department of Earth Atmospheric and Planetary Sciences, Massachusetts Institute of Technology, Cambridge, Massachusetts, USA, [3]Institute for the Study of Earth, Oceans, and Space, University of New Hampshire, Durham, New Hampshire, USA, [4]Los Alamos National Laboratory, Los Alamos, New Mexico, USA, [5]Laboratory of Atmospheric and Space Physics, University of Colorado Boulder, Boulder, Colorado, USA

**Abstract** This study is focused on understanding the coupling between different electron populations in the inner magnetosphere and the various physical processes that determine evolution of electron fluxes at different energies. Observations during the 17 March 2013 storm and simulations with a newly developed Versatile Electron Radiation Belt-4D (VERB-4D) are presented. Analysis of the drift trajectories of the energetic and relativistic electrons shows that electron trajectories at transitional energies with a first invariant on the scale of ~100 MeV/G may resemble ring current or relativistic electron trajectories depending on the level of geomagnetic activity. Simulations with the VERB-4D code including convection, radial diffusion, and energy diffusion are presented. Sensitivity simulations including various physical processes show how different acceleration mechanisms contribute to the energization of energetic electrons at transitional energies. In particular, the range of energies where inward transport is strongly influenced by both convection and radial diffusion are studied. The results of the 4-D simulations are compared to Van Allen Probes observations at a range of energies including source, seed, and core populations of the energetic and relativistic electrons in the inner magnetosphere.

## 1. Introduction

The dynamic evolution of the inner magnetosphere is primarily driven by the solar wind. However, predicting and understanding the nonlinear response of different electron populations in the inner magnetosphere, including ring current and higher energy radiation belts, has been a grand challenge since the beginning of the space age. The response of the radiation belts to solar variability is still poorly understood. *Reeves et al.* [2003] showed that approximately half of all geomagnetic storms result in a net depletion of the outer radiation belt or do not substantially change relativistic electron fluxes as compared to prestorm conditions, while the remaining 50% result in a net flux enhancement. Leading mechanisms for electron acceleration to relativistic energies include radial diffusion driven by ultralow frequency (ULF) waves [e.g., *Kellogg*, 1959; *Roederer*, 1970; *Fälthammar*, 1965; *Schulz and Lanzerotti*, 1974; *Hudson et al.*, 2001; *Elkington et al.*, 2003; *Shprits and Thorne*, 2004], local stochastic acceleration driven by very low frequency (VLF) or extremely low frequency (ELF) waves (see reviews by *Shprits et al.* [2008a, 2008b], *Millan and Thorne* [2007], *Millan and Baker* [2012], and references therein), and shock-induced acceleration [*Blake et al.*, 1992; *Li et al.*, 1993].

During this past decade, there have been a number of simulations of electron radiation belts ranging in complexity from 1-D [*Shprits et al.*, 2005, 2006; *Lam et al.*, 2009; *Chu et al.*, 2010] radial diffusion, and 2-D simulations of pitch angle and energy scattering [*Albert and Young*, 2005; *Shprits et al.*, 2006] to comprehensive 3-D short-term and long-term simulations [e.g., *Shprits et al.*, 2008a, 2008b; *Subbotin and Shprits*, 2009; *Subbotin et al.*, 2010, 2011a, 2011b; *Xiao et al.*, 2010; *Kim et al.*, 2011, 2012; *Kim and Shprits*, 2013; *Tu et al.*, 2013; *Glauert et al.*, 2014]. However, all of these simulations specified the outer boundary for the radial diffusion near GEO and also specified the lower energy boundary condition at all radial distances. These boundary conditions served as a source of particles that can be further accelerated to relativistic energies. The 3-D Fokker-Planck type codes accounted for the radial diffusion, pitch angle scattering, energy diffusion, and mixed pitch angle energy diffusion but ignored the convective transport that determines the dynamics of lower energy electrons.

There have also been a number of recent studies that focused on the dynamics of the lower energy ring current population, which is dominated by convective transport and losses. Historically, ring current studies concentrated on the dynamics of ions, as they contribute roughly 75 to 85% of the total energy density [*Frank*, 1967; *Liu et al*., 2005], while the dynamics of the ring current electrons have been largely neglected.

Several efforts have been recently made to combine convective transport with radial diffusion [e.g., *Miyoshi et al*., 2003] or convective transport, variable on short time scales with pitch angle scattering and energy diffusion but excluding radial diffusion due to ULF waves [e.g., *Fok et al*., 2014]. Particle tracing codes [e.g., *Hudson et al*., 2014, 2015; *Elkington et al*., 2002; *Kress et al*., 2014] allow for explicit modeling of radial diffusive and nondiffusive transport due to waves and convective transport due to global electric field but ignore local acceleration and use parameterized loss models.

In this study we first present observations of Van Allen Probes during March 2013 that illustrate the difference in the dynamics of various electron populations in the inner magnetosphere. We also present the analysis of electron drift trajectories at various energies with a focus on transitional energies. A qualitative comparison of the VERB-4D simulations with Van Allen Probes observations is also presented.

## 2. Observations of the 17 March 2013 Storm

In this study we focus on observations and modeling of the 17 March 2013 storm. Some aspects of this storm have been previously discussed by *Foster et al*. [2014] and *Baker et al*. [2014]. Examining individual satellite passes, *Foster et al*. [2014] noticed that during the 17 March storm, significant acceleration of 50 keV to 500 keV occurred at 22:17 UT. They also noticed that the plasmapause was depleted down to $L^*$ of 3.5 to 4.5. *Baker et al*. [2014] presented dynamics of the 2.8 to 7.2 MeV fluxes over the entire month of March 2013. They noticed that early March 2013 acceleration of ultrarelativistic electrons was associated with a gradual inward radial diffusion caused by a high-speed solar wind stream. They noticed that the solar eruption of the Active Region 1692 on the Sun produced a Class M.1 X-ray flare at 0650 UT on 15 March, which caused the rapid depletion of ultrarelativistic electrons down to low L shells. Pitch angle distributions at 2.8 MeV indicated that the loss to the magnetopause [*Shprits et al*., 2006] likely contributed to this depletion. Stronger dropouts were observed at higher energy [*Baker et al*., 2014]. After the storm, the fluxes of ultrarelativistic electrons rapidly recovered for the entire outer belt.

Due to the difference in dominant acceleration and loss processes, the dynamics of the inner magnetospheric electrons are strongly energy dependent. Figure 1 shows profiles of the electron flux evolution at four different energies ranging from ring current to ultrarelativistic, observed by Van Allen Probes A and B in March 2013.

There are distinct features in the evolution of the radial profiles of fluxes depending on the electron energy. During the storm main phase when *Kp* is large and *Dst* is strongly negative (−132 nT), electron fluxes at ring current energies of 50 keV and 200 keV are enhanced down to the inner zone. Even during weaker storms and intensifications of activity as indicated by increased *Kp*, 50 keV fluxes show rapid intensifications that decay on time scales of a few days or less. 200 keV particles show less variability but still respond to the storm on 1 March, 21 March, and 29 March.

While the division between the convection-dominated and radial diffusion-dominated inward transport has been customary and convenient, there is, of course, no sharp boundary between these electron populations. The fluxes of relativistic 1 MeV and ultrarelativistic 4.2 MeV electrons are not significantly injected by convection and drift around the Earth due to curvature and gradient drift and show quite different dynamics. Relativistic and ultrarelativistic fluxes show dropouts during the 17 March storm and then become enhanced over several days during the recovery phase.

As recently suggested by *Shprits et al*. [2013], ultrarelativistic energy electrons form a different population of particles where scattering by hiss is weaker and scattering by electromagnetic ion cyclotron (EMIC) waves plays a crucial role. Simulations also show that EMIC waves play an important role for the quiet time decay of the ultrarelativistic electron dynamics [*Drozdov et al*., 2015]. The difference in physical processes explains the unusual special structures often seen at ultrarelativistic energies [e.g., *Baker et al*., 2013, 2014] that persist for a long time.

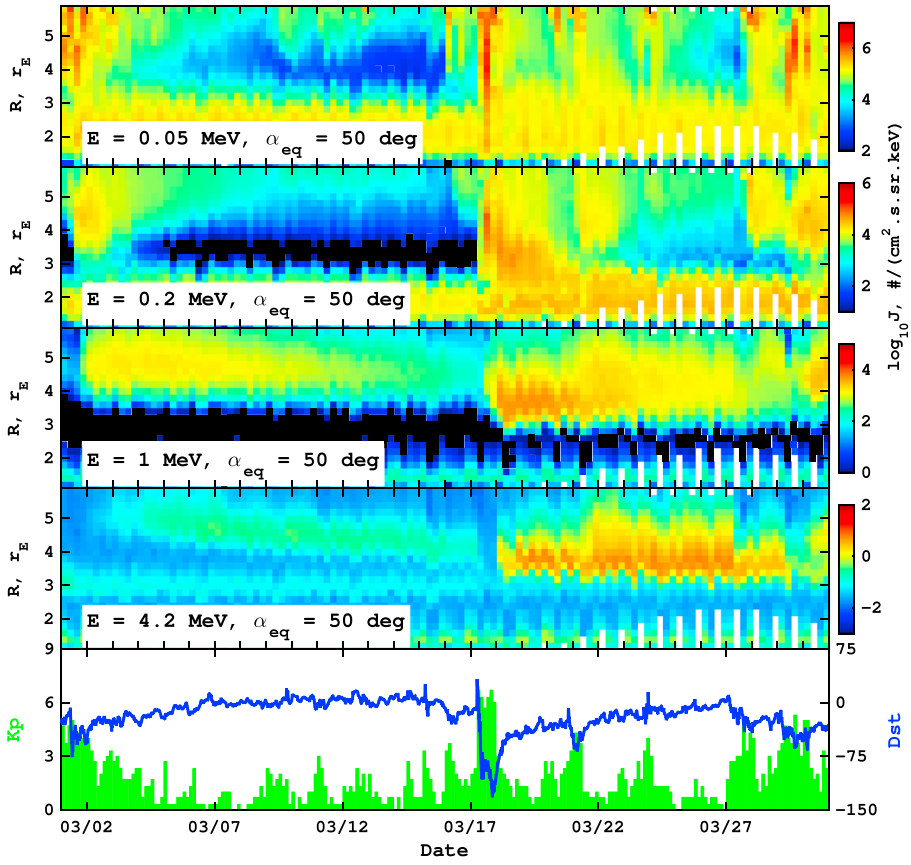


**Figure 1.** Dynamics of the electron flux evolution during March 2013, at 50 keV, 200 keV, 1 MeV observed by The Magnetic Electron Ion Spectrometer (MAGEIS) instrument, and 4.2 MeV observed by The Relativistic Electron-Proton Telescope (REPT) instrument on Van Allen Probes A and B. Dynamic evolution of energetic and relativistic radial electron flux profiles is illustrated. Different plasma populations clearly respond differently to the solar wind disturbances that are reflected in the *Kp* and *Dst* indices at the bottom.

There are clear differences in the evolution of ultrarelativistic and relativistic fluxes during March 2013. The dropouts extend to lower L shells and are more pronounced at ultrarelativistic energies. During 2 weeks before the 17 March storm, relativistic fluxes show a slowly decaying peak at a constant radial distance of approximately 4.5 $R_E$, while ultrarelativistic electrons show the split structure as during the September, 2012 storm and the inner edge of the outer belt clearly indicate the dominance of the inward radial diffusion during that time period.

## 3. Drift Trajectories

Figure 2 illustrates the difference in convective transport between the lower energy and higher energy electrons. Bounce-averaged drift velocities are calculated following *Roederer* [1970]:

$$<\mathbf{V}>_{ba} = \frac{\sqrt{8mc^2\mu}}{cq\tau_b B_0}\nabla_0 \boldsymbol{K}\times\boldsymbol{e}_0 + \frac{\boldsymbol{E}\times\boldsymbol{e}_0}{qB_0}, \quad (1)$$

where $\tau_b$ is bounce period, $\boldsymbol{B_0}$ is a background magnetic field, $\boldsymbol{e}_0 = \boldsymbol{B_0}/B_0$, $c$ is speed of light, $q$ is electron charge, $m$ is electron rest mass, $\mu$ is first adiabatic invariant, $E$ is the electric field, and $K$ = second adiabatic invariant. Index 0 refers to the value in the equatorial plane, and all variables are in the SI system. We use the Volland-Stern electric field model with a parameterization of *Maynard and Chen* [1975] and dipole magnetic field model.

At lower energy, the electron streamlines are close to the equipotential lines, and electrons are crossing L shells, being injected inward on the nightside and leaving the inner L shells on the dayside. At higher energies (e.g., >1000 MeV/G), electron transport is dominated by the curvature and gradient drifts. In a dipole field, most energetic electrons would undergo almost circular motion, and radial transport is dominated

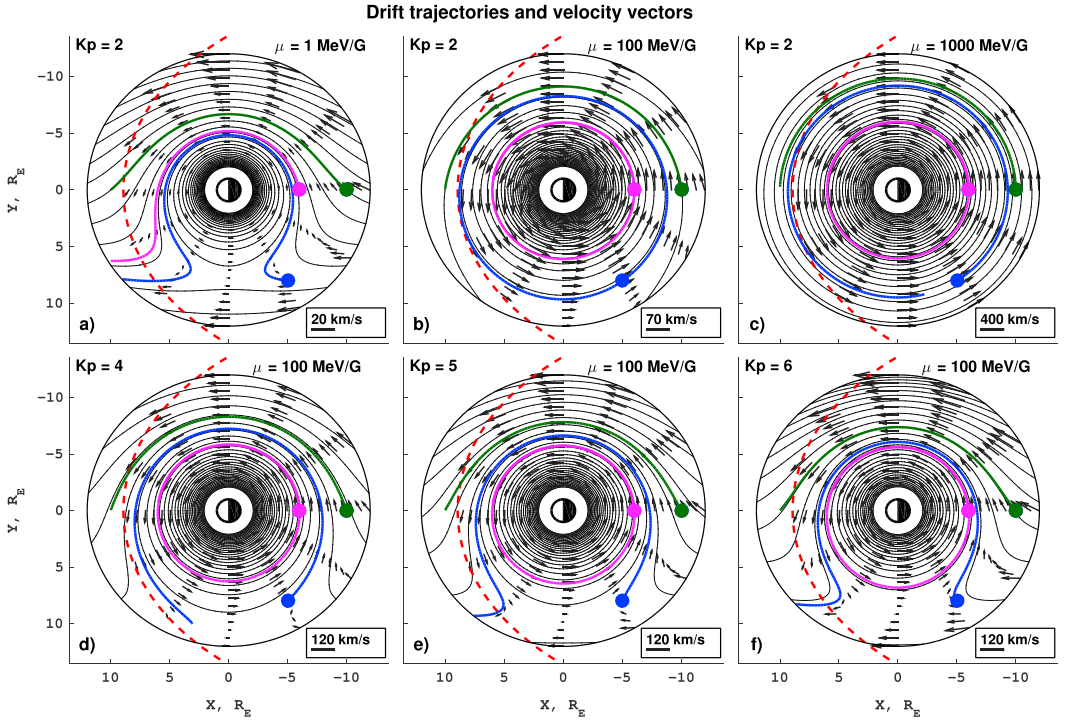


**Figure 2.** Trajectories of electrons at different values of the first invariant: (a) 1 MeV/G, (b) 100 MeV/G, and (c) 1000 MeV/G, and for 100 MeV/G particles three different *Kp* values: (d) $Kp = 4$, (e) $Kp = 5$, and (f) $Kp = 6$. The red dashed line indicates the location of the magnetopause [*Shue et al.*, 1997], assuming the magnitude of the interplanetary magnetic field of $B_z = -2$ nT and solar wind dynamic pressure of = 2 nPa. The colored solid lines indicate the trajectory of three different electrons, from a starting position indicated by the filled circles. The black arrows show the velocity direction of electrons for a given value of the adiabatic invariant, overlaid on contours of motion.

by the radial displacements due to the fluctuations of magnetic and electric field that are commonly modeled as a radial diffusion process. During relatively quiet geomagnetic conditions, 100 MeV/G electrons show nearly circular motion resembling the trajectories of relativistic electrons. However, as geomagnetic activity increases, the effects of the convection electric field become more pronounced, and trajectories bend to get close to the equipotential lines. In the next section we describe simulations of convection and radial diffusion, together with pitch angle and energy diffusion by VLF waves and show that electrons at intermediate values of the first adiabatic invariant can be transported by both convective transport and radial diffusion.

## 4. Convective and Diffusive Simulations

Currently, most of the 3-D Fokker-Planck diffusion codes [e.g., *Su et al.*, 2011; *Tu et al.*, 2013; *Glauert et al.*, 2014] follow the two-grid approach of *Subbotin and Shprits* [2009]. In this approach, radial diffusion simulations were done on a grid of constant adiabatic invariants, while pitch angle and energy simulations were done on a grid which is orthogonal in pitch angle and energy. Recently, *Subbotin and Shprits* [2012] suggested performing 3-D simulations on one grid of modified adiabatic invariants. This approach allows the elimination of interpolation between the numerical grids which can either lead to numerical errors or, in the case of accurate spline interpolation, cause unstable behavior of the code. The one-grid approach of *Subbotin and Shprits* [2012] can be easily augmented to include a fourth variable, $\varphi$, which is magnetic local time (MLT), and add another operator responsible for convection.

In this formulation, the evolution of four-dimensional Phase Space Density (PSD) *f* is solved in terms of radial distance, MLT, and the first and second adiabatic invariants:

$$\frac{df}{dt} = \langle v_\varphi \rangle \frac{\partial f}{\partial \varphi} + \langle v_R \rangle \frac{\partial f}{\partial R} + \frac{1}{G}\frac{\partial}{\partial L} G \langle D_{LL} \rangle \frac{\partial f}{\partial L} + \frac{1}{G}\frac{\partial}{\partial V} G \left( \langle D_{VV} \rangle \frac{\partial f}{\partial V} + \langle D_{VK} \rangle \frac{\partial f}{\partial K} \right) + \frac{1}{G}\frac{\partial}{\partial K} G \left( \langle D_{KV} \rangle \frac{\partial f}{\partial V} + \langle D_{KK} \rangle \frac{\partial f}{\partial K} \right) - \frac{f}{\tau} \quad (2)$$

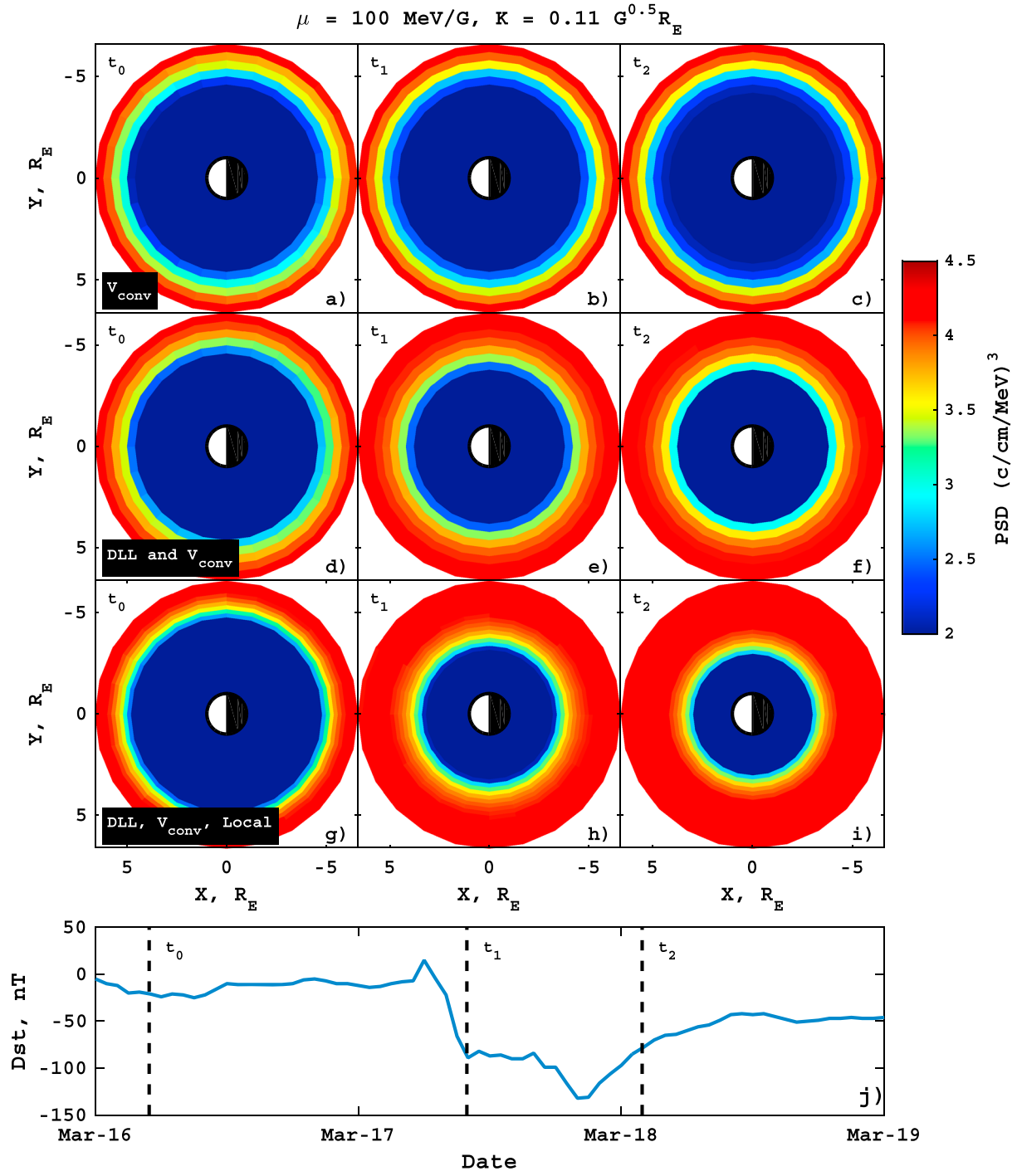


**Figure 3.** Simulations of $\mu = 100$ MeV/G, $K = 0.11\ G^{0.5}\ R_E$ electrons starting from an empty magnetosphere as an initial condition. A constant boundary condition is used at the outer boundary, see text for details. (a–c) Simulations using only convection, (d–f) simulations with convection and radial diffusion, (g–i) simulations with convection, radial diffusion, and local diffusion, and (j) *Dst* for a period during March 2013. Columns correspond to snapshots of the electron PSD as shown in Figure 3j.

where $\varphi$ is magnetic local time (MLT); $R$ is radial distance from the Earth; $L \equiv 2 \cdot \pi \cdot B_e/\Phi$ (this form of the third invariant is often denoted as $L^*$) is inversely proportional to the third adiabatic invariant $\Phi$; $B_e$ is the magnetic field at Earth's surface; $K = J/(8 \cdot \mu \cdot m_0)^{1/2}$, where $J$ is the second adiabatic invariant, $V \equiv \mu/(K + 0.5)^2$, where $\mu$ is the first adiabatic invariant; $<v_\varphi>$ and $<v_R>$ are bounce-averaged drift velocities; $<D_{LL}>$ $<D_{VV}>$, $<D_{KK}>$, and $<D_{VK}>$ are bounce-averaged diffusion coefficients; $G = (8 \cdot \mu \cdot m_0 \cdot c^2)^{1/2}/(K + 0.5)^2/L^2$ is the Jacobian of

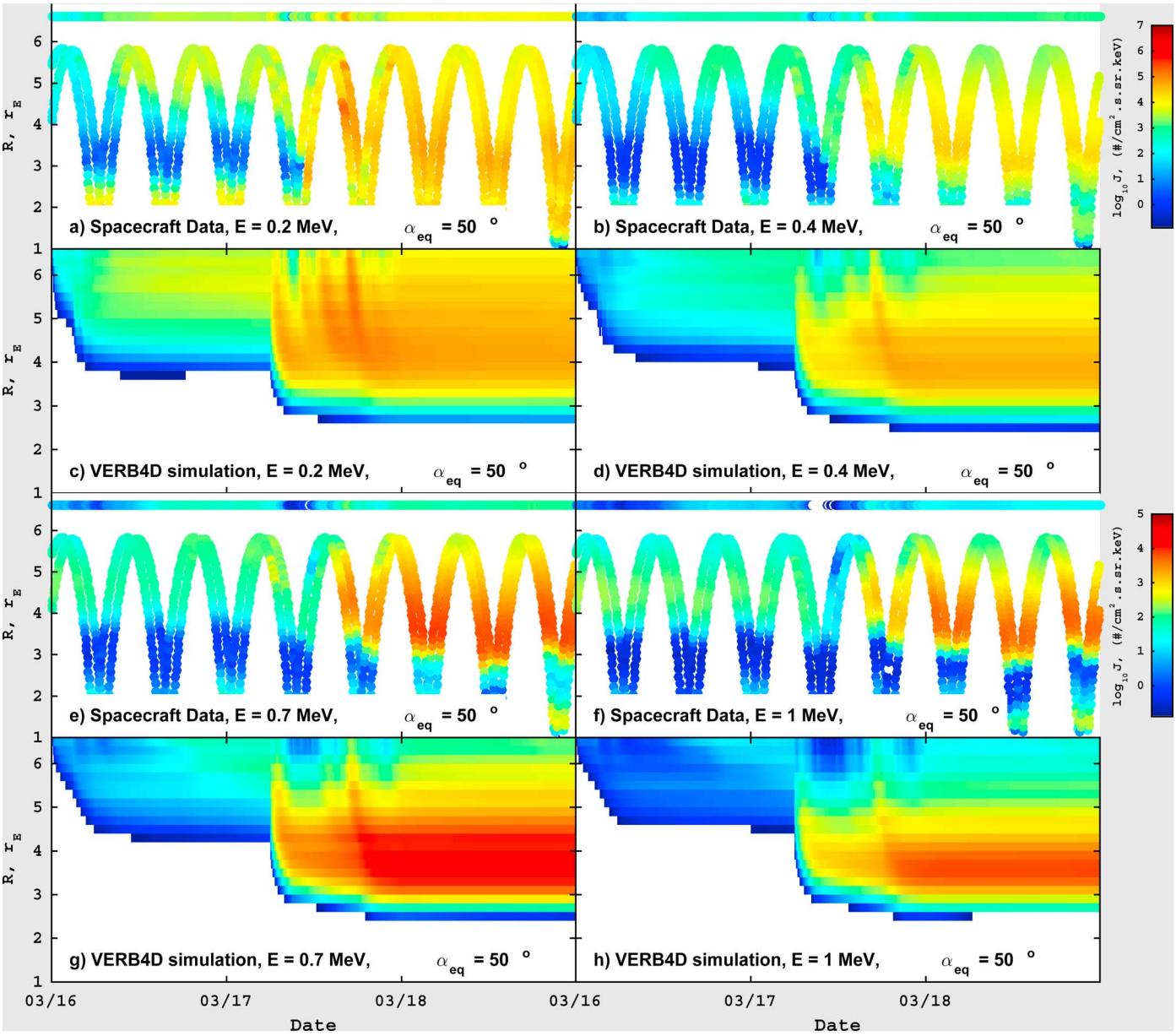


**Figure 4.** Radial fluxes as a function of time at a number of fixed energies and at an equatorial pitch angle of 50°. (a, b, e, and f) Van Allen Probes A and B spacecraft MAGEIS observations and GOES 13 and GOES 15 observed fluxes at $E = 0.1$, 0.4, 0.7, and 1.0 MeV, respectively. (c, d, g, and h) VERB-4D simulations of the evolution of fluxes at $E = 0.1$, 0.4, 0.7, and 1.0 MeV, respectively.

the transformation from an adiabatic invariant system ($\mu$, $J$, $\Phi$); and $f/\tau$, where $\tau$ represents the electron's lifetime losses. $V$ and $K$ are convenient for numerical calculations because $K$ is independent of the particle's energy and $V$ depends weakly on the particle's pitch angle. To compute radial transport, we will use the radial diffusion rates of *Brautigam and Albert* [2000].

The boundary condition is periodic in MLT. The inner boundary of the code is set at 1 $R_E$, where the phase space density is assumed to be zero due to the loss to the atmosphere. The outer boundary is set up for 10 keV to 10 MeV at $L = 6.6$, which allows for modeling a range of energies from tens of keV to multi-MeV in the heart of the radiation belts. In the simulation presented in Figure 3, the boundary spectrum is taken from *Subbotin et al.* [2011b] and based on an average flux spectrum from long-term observations on Polar and CRRES. The boundary is kept constant for the duration of that simulation.

Figure 3 shows sensitivity simulations using constant outer boundary condition and including convection only (a–c); convection and radial diffusion (d–f); and convection, radial diffusion, pitch angles, energy, and mixed energy-pitch angle diffusion. Simulations with convection only during quiet and disturbed geomagnetic conditions do not allow for significant injections of particles into the inner regions. Addition of radial diffusion results in injection down to $L = 4$. Inclusion of the local acceleration and loss due to chorus waves shows a gradual increase in fluxes in the recovery phase of the storm.

Figure 4 shows a comparison of Van Allen Probes observations with VERB-4D simulations at various energies. For this simulation, the boundary conditions are set up at the radial distance $R_0 = 6.6\,R_E$ according to GOES 13 and GOES 15 measurements. GOES 13 and GOES 15 observations are taken at a 6 min cadence and averaged. The fluxes as a function of energy are first fitted to a power law which is used to interpolate between values up to 1 MeV. We extrapolate using a nearest approach to lower energies as the flux spectrum begins to flatten out near 30 keV. We use an exponential fit to interpolate and extrapolate to fluxes above 1 MeV. The EPEAD integral channels are fitted to an exponential in order to compute differential fluxes. The pitch angle distribution below 500 keV is directly measured, which allows us to fit a functional form over the data in order to cover all equatorial pitch angles. The fit takes two forms: for monotonically increasing flux with pitch angle, we apply a sine fit up to the fourth order to extend the fit to 90°. A constraint based on absolute deviation restricts the fitted function and reverts to a simple sine fit if no solution is found. For butterfly distributions, we simply perform a nearest extrapolation from the highest measured pitch angle to 90°. The flux data are then converted to PSD in invariant $V$ and $K$ coordinates and gridded to the model using a nearest neighbor approach. The PSD at minimum $V$ from GOES is then used to scale the lower $V$ boundary at points inward of the outer boundary using a steady state solution to the radial diffusion equation. For this initial study, we used a dipole field model to infer phase space density at GEO. Clearly visible are periodic variations in boundary fluxes at all energies, including fluxes at relativistic energies which are associated with the inaccuracies of the dipole field. The boundary conditions are discussed in more detail in the supporting section.

At the lowest presented energy of 200 keV, the Van Allen Probes observations show an increase in fluxes during 17 March and decay right after the main phase of the storm. In general, the model describes a similar evolution to the observed fluxes and reproduces the increase in fluxes down to $L = 4$ with a peak around $L = 5$. However, the model predicts an earlier increase than is seen in the observations, most likely due to the difference in MLT between the GOES spacecraft that is used for boundary conditions and Van Allen Probes observations. At 400 keV, a visible increase in fluxes starts in the afternoon of 17 March and persists longer than for a 200 keV stormtime increase, with a peak at approximately $L = 4$. Noticeable in the data and model are an increase in the area of intense fluxes during the recovery phase, indicative of the biradial transport of particles. At higher energies, the electron fluxes show similar dynamics with a prolonged recovery and peak at around $L = 4$. The values of the poststorm increase predicted by VERB-4D are very similar to the observed values by Van Allen Probes. The differences between the simulations and models are most likely due to the simplified boundary conditions and neglected adiabatic variations. The results of the model are only visually compared with data and not quantitatively, which is left for future and more detailed studies. Current simulations also do not include simulations of the ultrarelativistic electrons, as such simulations require inclusion of the EMIC waves to reproduce stormtime dropouts [*Shprits et al.*, 2013] and quiet time decay rates [*Drozdov et al.*, 2015].

## 5. Summary

Observations of the evolution of fluxes during March 2013 clearly demonstrate that energetic, relativistic, and ultrarelativistic electrons show very different dynamics. Modeling of the dynamics of these electron populations with a single code that combines all the relevant physical processes is a challenging task. The dynamics of energetic electrons are dominated by convective transport and loss, while at relativistic and ultrarelativistic energies, the dynamics are dominated by radial transport, local acceleration, and loss. Analysis of the drift trajectories of the energetic and relativistic electrons shows that electron trajectories at transitional energies with the first invariant on the scale of ~100 MeV/G may resemble ring current or relativistic electron trajectories, depending on the level of geomagnetic activity. Sensitivity simulations with VERB-4D show that electrons with transitional values of the first adiabatic invariant (~100 MeV/G) are simultaneously affected by convective and diffusive transport. While convective transport provides injections around geosynchronous orbit, radial diffusion and local acceleration due to energy diffusion

allow for further acceleration in the heart of the radiation belts and provide the source population for the relativistic electrons and seed population for chorus waves.

The detailed comparison with observations at various energies can help validate the code and reveal the dominant physical mechanisms. Four-dimensional simulations show similar dynamics as observations with noted differences are likely due to inaccuracies in the boundary conditions, as well as neglect of the realistic magnetic field and adiabatic variations. The direct comparison is complicated by the fact that GOES observes fluxes only at a particular MLT. Future modeling will include more comprehensive boundary conditions, a realistic magnetic field, adiabatic variations, loss to the magnetopause, and more realistic models of the electric field. Modeling in the realistic field will also allow for estimation of the loss to the magnetopause and the outward transport that will be caused by the inward gradient in phase space density. We will also be able to explore if additional transport (e.g., due to localized electric field) is required to explain the dynamics of the ring current electrons. Simulations with the VERB-4D code will allow comparison of simulations at various MLT with multipoint observations provided by constellations of Van Allen Probes, Time History of Events and Macroscale Interactions during Substorms (THEMIS), Cluster II, Magnetospheric Multiscale (MMS), and other missions.

**Acknowledgments**

We would like to thank UCLA programmer Dmitri Subbotin for his contributions to the development of the VERB code. We would like to thank UCLA undergraduate students Josh Adler and Alec Jen who worked on testing, validating, and documenting the code. We would also like to thank Michael Schulz, Richard Thorne, Paul O'Brien, and Mary Hudson for useful discussion. This research was supported by NASA awards NNX10AK99G and NNX13AE34G, NSF award AGS-1243183, UC Lab Fee award 116720, and Horizon 2020 award 637302. We would like to thank ECT and EMFISIS Van Allen Probes teams for providing data which is publically available at the JHU/APL website.

The Editor thanks two anonymous reviewers for their assistance in evaluating this paper.

## References

Albert, J., and S. Young (2005), Multidimensional quasi-linear diffusion of radiation belt electrons, *Geophys. Res. Lett.*, *32*, L14110, doi:10.1029/2005GL023191.

Baker, D. N., et al. (2013), A long-lived relativistic electron storage ring embedded in Earth's outer Van Allen belt, *Science*, *340*, 186–190, doi:10.1126/science.1233518.

Baker, D. N., et al. (2014), Gradual diffusion and punctuated phase space density enhancements of highly relativistic electrons: Van Allen Probes observations, *Geophys. Res. Lett.*, *41*, 1351–1358, doi:10.1002/2013GL058942.

Blake, J. B., W. A. Kolasinski, R. W. Fillius, and E. G. Mullen (1992), Injection of electrons and protons with energies of tens of MeV into $L<3$ on 24 March 1991, *Geophys. Res. Lett.*, *19*, 821–824, doi:10.1029/92GL00624.

Brautigam, D., and J. Albert (2000), Radial diffusion analysis of outer radiation belt electrons during the October 9, 1990, magnetic storm, *J. Geophys. Res.*, *105*(A1), 291–309, doi:10.1029/1999JA900344.

Chu, F., M. K. Hudson, P. Haines, and Y. Shprits (2010), Dynamic modeling of radiation belt electrons by radial diffusion simulation for a 2 month interval following the 24 March 1991 storm injection, *J. Geophys. Res.*, *115*, A03210, doi:10.1029/2009JA014409.

Drozdov, A. Y., Y. Y. Shprits, K. G. Orlova, A. C. Kellerman, D. A. Subbotin, D. N. Baker, H. E. Spence, and G. D. Reeves (2015), Energetic, relativistic and ultra-relativistic electrons: Comparison of long-term VERB code simulations with Van Allen Probes measurements, *J. Geophys. Res. Space Physics*, *120*, 3574–3587, doi:10.1002/2014JA020637.

Elkington, S. R., M. K. Hudson, M. J. Wiltberger, and J. G. Lyon (2002), MHD/particle simulations of radiation belt dynamics, *J. Atmos. Sol. Terr. Phys.*, *64*(5), 607–615.

Elkington, S. R., M. K. Hudson, and A. A. Chan (2003), Resonant acceleration and diffusion of outer zone electrons in an asymmetric geomagnetic field, *J. Geophys. Res.*, *108*(A3), 1116, doi:10.1029/2001JA009202.

Fälthammar, C.-G. (1965), Effects of time-dependent electric fields on geomagnetically trapped radiation, *J. Geophys. Res.*, *70*(11), 2503–2516, doi:10.1029/JZ070i011p02503.

Fok, M.-C., N. Y. Buzulukova, S.-H. Chen, A. Glocer, T. Nagai, P. Valek, and J. D. Perez (2014), The comprehensive inner magnetosphere-ionosphere model, *J. Geophys. Res. Space Physics*, *119*, 7522–7540, doi:10.1002/2014JA020239.

Foster, J. C., et al. (2014), Prompt energization of relativistic and highly relativistic electrons during a substorm interval: Van Allen Probes observations, *Geophys. Res. Lett.*, *41*, 20–25, doi:10.1002/2013GL058438.

Frank, L. (1967), On the extraterrestrial ring current during geomagnetic storms, *J. Geophys. Res.*, *72*, 3753–3767, doi:10.1029/JZ072i015p03753.

Glauert, S. A., R. B. Horne, and N. P. Meredith (2014), Three-dimensional electron radiation belt simulations using the BAS Radiation Belt Model with new diffusion models for chorus, plasmaspheric hiss, and lightning-generated whistlers, *J. Geophys. Res. Space Physics*, *119*, 268–289, doi:10.1002/2013JA019281.

Hudson, M. K., et al. (2001), Radiation belt electron acceleration by ULF wave drift resonance: Simulation of 1997 and 1998 storms, in *Space Weather*, *AGU Monogr.*, vol. 125, edited by P. Song, H. Singer, and G. Siscoe, 289 pp., AGU, Washington, D. C.

Hudson, M. K., D. N. Baker, J. Goldstein, B. T. Kress, J. Paral, F. Toffoletto, and M. Wiltberger (2014), Simulated magnetopause losses and Van Allen Probe flux dropouts, *Geophys. Res. Lett.*, *41*, 1113–1118, doi:10.1002/2014GL059222.

Hudson, M. K., J. Paral, B. T. Kress, M. Wiltberger, D. N. Baker, J. C. Foster, D. L. Turner, and J. R. Wygant (2015), Modeling CME-shock-driven storms in 2012–2013: MHD test particle simulations, *J. Geophys. Res. Space Physics*, *120*, 1168–1181, doi:10.1002/2014JA020833.

Kellogg, P. J. (1959), Van Allen radiation of solar origin, *Nature*, *183*, 1295–1297.

Kim, K.-C., and Y. Y. Shprits (2013), Long-term relativistic radiation belt electron responses to GEM magnetic storms, *J. Atmos. Sol. Terr. Phys.*, *100–101*, 59–67.

Kim, K.-C., Y. Shprits, D. Subbotin, and B. Ni (2011), Understanding the dynamic evolution of the relativistic electron slot region including radial and pitch angle diffusion, *J. Geophys. Res.*, *116*, A10214, doi:10.1029/2011JA016684.

Kim, K.-C., Y. Shprits, D. Subbotin, and B. Ni (2012), Relativistic radiation belt electron responses to GEM magnetic storms: Comparison of CRRES observations with 3-D VERB simulations, *J. Geophys. Res.*, *117*, A08221, doi:10.1029/2011JA017460.

Kress, B. T., M. K. Hudson, and J. Paral (2014), Rebuilding of the Earth's outer electron belt during 8–10 October 2012, *Geophys. Res. Lett.*, *41*, 749–754, doi:10.1002/2013GL058588.

Lam, M. M., R. B. Horne, N. P. Meredith, and S. A. Glauert (2009), Radiation belt electron flux variability during three CIR-driven geomagnetic storms, *J. Atmos. Sol. Terr. Phys.*, *71*, 1145–1156.

Li, X., I. Roth, M. Temerin, J. R. Wygant, M. K. Hudson, and J. B. Blake (1993), Simulation of the prompt energization and transport of radiation belt particles during the March 24, 1991 SSC, *Geophys. Res. Lett.*, *20*(22), 2423–2426.

Liu, S., M. W. Chen, J. L. Roeder, L. R. Lyons, and M. Schulz (2005), Relative contribution of electrons to the stormtime total ring current energy content, *Geophys. Res. Lett.*, *32*, L03110, doi:10.1029/2004GL021672.

Maynard, N. C., and A. J. Chen (1975), Isolated cold plasma regions: Observations and their relation to possible production mechanisms, *J. Geophys. Res.*, *80*(7), 1009–1013, doi:10.1029/JA080i007p01009.

Millan, R. M., and D. N. Baker (2012), Acceleration of particles to high energies in Earth's radiation belts, *Space Sci. Rev.*, *173*(1–4), 103–131, doi:10.1007/s11214-012-9941-x.

Millan, R. M., and R. M. Thorne (2007), Review of radiation belt relativistic electron losses, *J. Atmos. Sol. Terr. Phys.*, *69*(3), 362–377, doi:10.1016/j.jastp.2006.06.019.

Miyoshi, Y., A. Morioka, H. Misawa, T. Obara, T. Nagai, and Y. Kasahara (2003), Rebuilding process of the outer radiation belt during the 3 November 1993 magnetic storm: NOAA and Exos-D observations, *J. Geophys. Res.*, *108*(A1), 1004, doi:10.1029/2001JA007542.

Reeves, G. D., K. L. McAdams, R. H. W. Friedel, and T. P. O'Brien (2003), Acceleration and loss of relativistic electrons during geomagnetic storms, *Geophys. Res. Lett.*, *30*(10), 1529, doi:10.1029/2002GL016513.

Roederer, J. G. (1970), *Dynamics of Geomagnetically Trapped Radiation*, Springer, New York.

Schulz, M., and L. J. Lanzerotti (1974), *Particle Diffusion in the Radiation Belts*, *Phys. Chem. Space*, vol. 7, 218 pp., Springer, New York, doi:10.1007/978-3-642-65675-0.

Shprits, Y. Y., and R. M. Thorne (2004), Time-dependent radial diffusion modeling of relativistic electrons with realistic loss rates, *Geophys. Res. Lett.*, *31*, L08805, doi:10.1029/2004GL019591.

Shprits, Y. Y., R. M. Thorne, G. D. Reeves, and R. Friedel (2005), Radial diffusion modeling with empirical lifetimes: Comparison with CRRES observations, *Ann. Geophys.*, *23*(4), 1467–1471.

Shprits, Y. Y., W. Li, and R. M. Thorne (2006), Controlling effect of the pitch angle scattering rates near the edge of the loss cone on electron lifetimes, *J. Geophys. Res.*, *111*, A12206, doi:10.1029/2006JA011758.

Shprits, Y. Y., S. R. Elkington, N. P. Meredith, and D. A. Subbotin (2008a), Review of modeling of losses and sources of relativistic electrons in the outer radiation belts: I. Radial transport, *J. Atmos. Sol. Terr. Phys.*, *70*(14), 1679–1693, doi:10.1016/j.jastp.2008.06.008.

Shprits, Y. Y., D. A. Subbotin, N. P. Meredith, and S. R. Elkington (2008b), Review of modeling of losses and sources of relativistic electrons in the outer radiation belts: II. Local acceleration and loss, *J. Atmos. Sol. Terr. Phys.*, *70*(14), 1694–1713, doi:10.1016/j.jastp.2008.06.014.

Shprits, Y. Y., D. Subbotin, A. Drozdov, M. E. Usanova, A. Kellerman, K. Orlova, D. N. Baker, D. L. Turner, and K.-C. Kim (2013), Unusual stable trapping of the ultrarelativistic electrons in the Van Allen radiation belts, *Nat. Phys.*, doi:10.1038/nphys2760.

Shue, J. H., J. Chao, H. Fu, C. Russell, P. Song, K. Khurana, and H. Singer (1997), A new functional form to study the solar wind control of the magnetopause size and shape, *J. Geophys. Res.*, *102*(A5), 9497–9511, doi:10.1029/97JA00196.

Su, Z., F. Xiao, H. Zheng, and S. Wang (2011), Radiation belt electron dynamics driven by adiabatic transport, radial diffusion, and wave-particle interactions, *J. Geophys. Res.*, *116*, A04205, doi:10.1029/2010JA016228.

Subbotin, D. A., and Y. Y. Shprits (2009), Three-dimensional modeling of the radiation belts using the Versatile Electron Radiation Belt (VERB) code, *Space Weather*, *7*, S10001, doi:10.1029/2008SW000452.

Subbotin, D. A., and Y. Y. Shprits (2012), Three-dimensional radiation belt simulations in terms of adiabatic invariants using a single numerical grid, *J. Geophys. Res.*, *117*, A05205, doi:10.1029/2011JA017467.

Subbotin, D. A., Y. Y. Shprits, and B. Ni (2011a), Long-term radiation belt simulation with the VERB 3-D code: Comparison with CRRES observations, *J. Geophys. Res.*, *116*, A12210, doi:10.1029/2011JA017019.

Subbotin, D. A., Y. Y. Shprits, M. Gkioulidou, L. R. Lyons, B. Ni, V. G. Merkin, F. R. Toffoletto, R. M. Thorne, R. B. Horne, and M. K. Hudson (2011b), Simulation of the acceleration of relativistic electrons in the inner magnetosphere using RCM-VERB coupled codes, *J. Geophys. Res.*, *116*, A08211, doi:10.1029/2010JA016350.

Subbotin, D., Y. Shprits, and B. Ni (2010), Three-dimensional VERB radiation belt simulations including mixed diffusion, *J. Geophys. Res.*, *115*, A03205, doi:10.1029/2009JA015070.

Tu, W., G. S. Cunningham, Y. Chen, M. G. Henderson, E. Camporeale, and G. D. Reeves (2013), Modeling radiation belt electron dynamics during GEM challenge intervals with the DREAM3D diffusion model, *J. Geophys. Res. Space Physics*, *118*, 6197–6211, doi:10.1002/jgra.50560.

Xiao, F., Z. Su, H. Zheng, and S. Wang (2010), Three-dimensional simulations of outer radiation belt electron dynamics including cross-diffusion terms, *J. Geophys. Res.*, *115*, A05216, doi:10.1029/2009JA014541.